# Particle–γ coincidences and coplanarity in the $^{32}S+^{24}Mg$ binary reaction

Wheldon, Carl; Kokalova, T; Vonoertzen, W; Gebauer, B; Bohlen, H; Schulz, C; Thummerer, S; Efimov, G; Beck, C; Curien, D

*DOI:*
10.1016/j.nuclphysa.2008.08.006

*Document Version*
Publisher's PDF, also known as Version of record

*Citation for published version (Harvard):*
Wheldon, C, Kokalova, T, Vonoertzen, W, Gebauer, B, Bohlen, H, Schulz, C, Thummerer, S, Efimov, G, Beck, C & Curien, D 2008, 'Particle–γ coincidences and coplanarity in the $^{32}S+^{24}Mg$ binary reaction', *Nuclear Physics A*, vol. 811, no. 3-4, pp. 276-290. https://doi.org/10.1016/j.nuclphysa.2008.08.006

Available online at www.sciencedirect.com
ScienceDirect
Nuclear Physics A 811 (2008) 276–290
NUCLEAR PHYSICS A
www.elsevier.com/locate/nuclphysa

# Particle–$\gamma$ coincidences and coplanarity in the $^{32}S + ^{24}Mg$ binary reaction

C. Wheldon [a,b,*], Tz. Kokalova [a], W. von Oertzen [a,c], B. Gebauer [a], H.G. Bohlen [a], Ch. Schulz [a], S. Thummerer [a], G. Efimov [d], C. Beck [e], D. Curien [e], P. Papka [e,1]

[a] *SF7, Hahn-Meitner-Institut, Glienicker Straße 100, D-14109 Berlin, Germany*
[b] *School of Physics and Astronomy, University of Birmingham, Edgbaston, B15 2TT, Birmingham, UK*
[c] *Fachbereich Physik, Freie Universität Berlin, Arnimallee 14, D-14195 Berlin, Germany*
[d] *Flerov Laboratory for Nuclear Reactions, Joint Institute for Nuclear Research, 141980 Dubna, Moscow region, Russian Federation*
[e] *Institut Pluridisciplinaire Hubert Curien—Département de Recherches Subatomiques, UMR7178, IN2P3-CNRS et Université Louis Pasteur (Strasbourg I), 23 Rue du Loess, B.P. 28, F-67037 Strasbourg cedex 2, France*

Received 1 April 2008; received in revised form 11 June 2008; accepted 6 August 2008

Available online 20 August 2008

**Abstract**

The reaction $^{32}S$ (165.4 MeV) + $^{24}Mg$ is studied using the binary reaction spectrometer (BRS) coupled to the EUROBALL Ge-detector array. Particle–particle–$\gamma$ and particle–$\gamma$–$\gamma$ coincidences have been examined together with $\gamma$–$\gamma$-only coincidences for the fusion-evaporation residues. Recent reports of evidence for hyper-deformation from angular correlations in similar data are investigated. Analogous out-of-plane angular correlations are observed but attributed to reactions with the target contaminants $^{16}O$ and $^{12}C$. This is consistent with the contamination observed in the $\gamma$–$\gamma$-only data.


*PACS:* 23.20.Lv; 25.70.Hi

*Keywords:* NUCLEAR REACTIONS $^{24}Mg(^{32}S, X)$, $E = 165.4$ MeV; measured $E_\gamma$, $I_\gamma$, $\gamma\gamma$-, (residue)$\gamma$-coincidence, reaction product yields; deduced reaction mechanism features and deformation. Doppler shift correction. Berlin binary reaction spectrometer and the Euroball IV array

* Corresponding author at: School of Physics and Astronomy, University of Birmingham, Edgbaston, B15 2TT, Birmingham, UK.
*E-mail address:* c.wheldon@bham.ac.uk (C. Wheldon).
[1] Present address: iThemba Labs, PO Box 722, Somerset West 7129, South Africa.

0375-9474/$ – see front matter 
doi:10.1016/j.nuclphysa.2008.08.006

## 1. Introduction

Recent results have been published claiming evidence for the observation of hyper-deformation in $^{60}$Zn based on the interpretation of particle–particle coincidences following the binary reactions between $^{36}$Ar at 195 MeV and a $^{24}$Mg target [1,2]. The analysis focused on the out-of-plane angular correlations. The work was carried out using a unique experimental system enabling the coincident measurement of particles (identified by $Z$) over a large angular range and $\gamma$ rays using an array of Ge detectors; the OSIRIS spectrometer [3]. The current work, presented here is of a similar nature, using the same large-area particle detector system, the Berlin Binary Reaction Spectrometer (BRS), but coupled to the much larger EUROBALL Ge array. The present experiment also made use of a $^{24}$Mg target but here the beam is $^{32}$S at 165.4 MeV leading to the compound nucleus $^{56}$Ni. Although the targets used in each measurement are similar, in the earlier $^{60}$Zn work use was made of a target-lock system to transfer the target to the chamber under vacuum, whereas for the $^{56}$Ni run the target was stored unprotected prior to the measurement. An additional feature of the current work is the availability of $\gamma$–$\gamma$ coincidences from EUROBALL without the accompanying particle triggers, providing access to the fusion-evaporation products and yielding two contrasting data sets from the same experiment. In light of the above mentioned similarities in the data it is worthwhile investigating the case for hyper-deformation. A separate analysis/interpretation of the present data, similar to that for the $^{60}$Zn data and considering only the particle information, is to appear as Ref. [4]. Although Ref. [4] has some common coauthors (due to participation/involvement in the experiment, etc.), the data-sorting, calibrations and analysis were carried out independently and differently from the current work.

## 2. Experimental method

An experiment was performed in April 2003 at the VIVITRON Tandem facility of the IReS at Strasbourg. A 165.4 MeV beam of 2–3 pnA, $^{32}$S ions was used to bombard a $2 \times 120$ μg cm$^{-2}$ $^{24}$Mg target, each foil being backed with 10 μg cm$^{-2}$ carbon. As mentioned above, the target was stored unprotected prior to the experiment, leading to significant oxidation. The target was located at the centre of the EUROBALL IV Ge detector array. In this case the array comprised 209 Ge-crystals: 15 cluster detectors at backward angles, each comprising 7 Ge crystals in one Compton suppression shield, and 25 clover detectors close to 90°, each comprising 4 Ge crystals within one suppression shield. The forward-angle tapered Ge detectors of EUROBALL were replaced by the two-arm BRS detector. This set-up [5,6] is shown in Fig. 1. Three trigger conditions were set, requiring:

(i) $\geqslant 2$ Ge detectors to fire;
(ii) $\geqslant 1$ BRS detector; or
(iii) $\geqslant 1$ BRS and $\geqslant 1$ Ge detector.

Typical rates for the three triggers were: (i) 11 kHz (94%); (ii) 500 Hz (4.3%); and (iii) 200 Hz (1.7%). Radioactive sources of $^{152}$Eu, $^{133}$Ba and $^{56}$Co at the target position were used to obtain energy and efficiency calibrations for the Ge detectors. Note that the last calibration point for the Ge crystals is therefore at 3.45 MeV. Beyond this, energies and efficiencies are extrapolated leading to increased uncertainties. However, the $^{16}$O peaks with published values of $6128.63 \pm 0.04$ and $6915.5 \pm 0.6$ keV are observed at $6130 \pm 3$ and $6920 \pm 6$ keV respectively, after performing the Doppler-shift correction. Similarly, the $^{12}$C, $4438.0 \pm 0.3$ keV energy [7] is measured

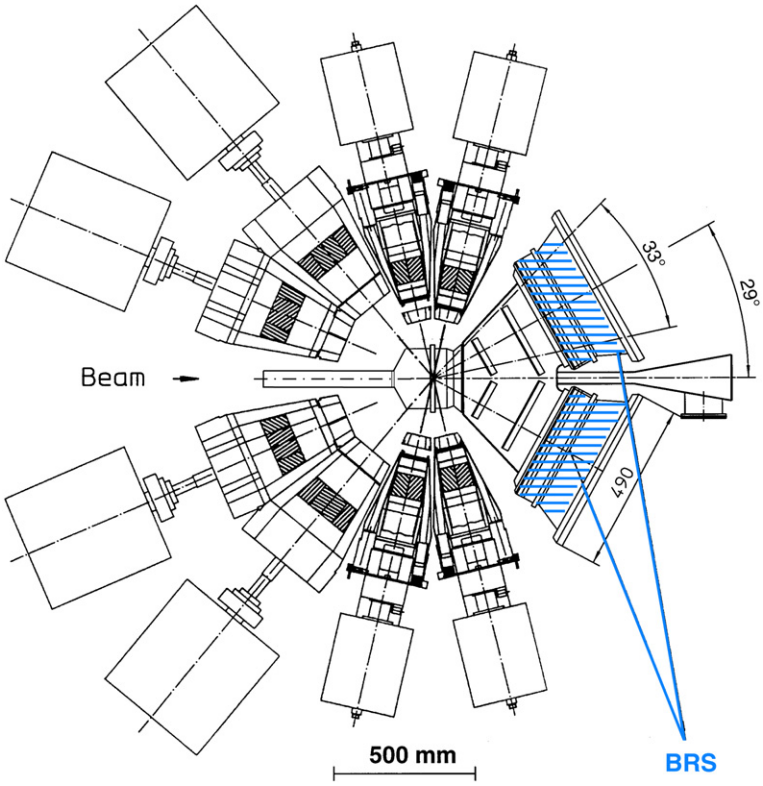


Fig. 1. Scale drawing showing the set-up of the BRS detectors at EUROBALL. The two BRS telescopes are stacked in a vertical configuration around the 0° beam axis. Close to 90° are the clover Ge detectors and at backward angles are the larger cluster Ge detectors.

here at $4437 \pm 2$ keV. Due to the large number of Ge crystals, the calibration was automated using a custom written routine [CW] based on the RadWare [8] analysis package. Output from the RadWare peak-finding routines was used to systematically calculate linear calibration coefficients by checking all possible pairs of identified peaks against all possible pairs of known source energies. These coefficients were then used to test the match between the remaining peaks and source energies not used in the calculation of the coefficients. The 'best fit' coefficients were taken which matched the largest number of source peaks having the lowest $\chi^2$. A similar procedure is used for the online calibration at the RISING setup at GSI [9].

## 3. Overview of the BRS

Here, a few details of the BRS detector system are given. The BRS was designed and built in Berlin by B. Gebauer et al. [5,6]. The complete technical specification will appear as Ref. [10]. Some details can also be found in Refs. [11–14].

The first stage of each BRS detector comprises a low-pressure multi-wire chamber (MWC) providing the position ($x$ and $y$) information for the incoming ions. The telescopes have rectangular cross-sections, widening conically from the MWCs to the second stage Bragg-curve ionisation chambers (BICs) and the mounting at EUROBALL (Fig. 1) was such that the centre of

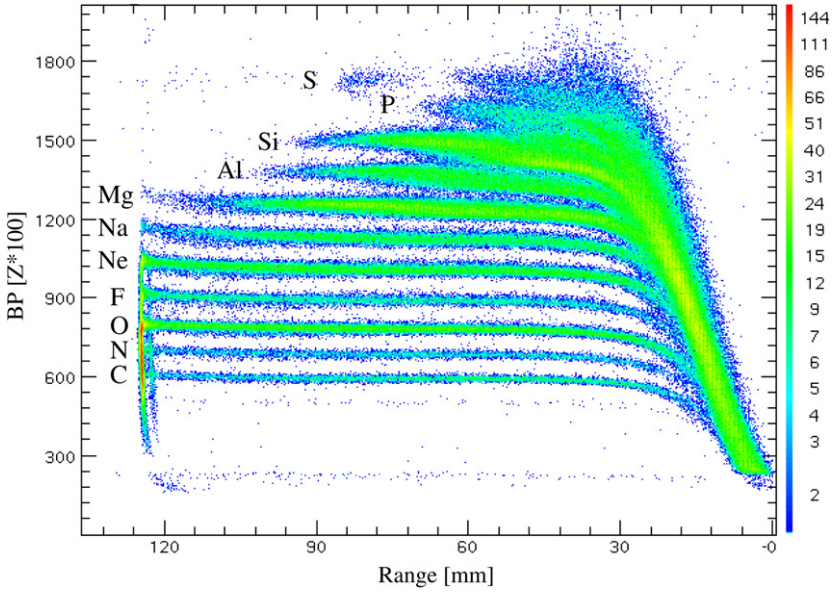


Fig. 2. A plot for telescope 2 showing range, $R$, versus Bragg peak, $BP$. Each horizontal line corresponds to a different atomic charge, $Z$, as labelled. The vertical axis is in units of $\approx Z \times 100$. The Bragg chamber is 125 mm deep. Relative intensity is shown on the side bar.

the front plane of each telescope was 361.6 mm from the target position. This results in angular ranges for each telescope of: $\theta = 12.5^\circ \rightarrow 45.5^\circ$ and $\phi = -16.5^\circ \rightarrow 16.5^\circ$. All detection planes of both detector stages are subdivided into four segments. From each of the four BIC segments per telescope, three signal types are derived:

(i) The Bragg-peak signal ($BP$), representing the maxima of the stopping (Bragg) curves of the reaction products in the counting gas. The $BP$ delivers $Z$ information.
(ii) The range signal ($R$), representing the range of ions in the active gas volume of the BIC (Fig. 2).
(iii) The energy signal ($E$), representing the kinetic energy of the ions after penetrating the MWC and the BIC entrance window.

### *3.1. Treatment of the BRS data*

Below, the treatment of the BRS data in the offline analysis is described.

The BRS positions were calibrated using elastic scattering data collected with a 210 $\mu g\,cm^{-2}$ $^{197}$Au target and using the known positions of slits in movable masks in front of the BRS telescopes. Events with good positions were used to define a BRS event as opposed to a EUROBALL-only event. From the position signals, the in-plane, $\theta$, and out-of-plane, $\phi$, angles are calculated. The BIC energy signals were calibrated using the end-point energies observed in the $E$ versus $BP$ plots (Fig. 3). The maximum kinetic energy deposited by the ions in the BIC was calculated using an energy-loss code, taking into account the window foils and gases. Following this procedure, the four segments could be summed together. (Note, that segment four of the first detector telescope could not be summed due to a different response profile, caused by a difference in

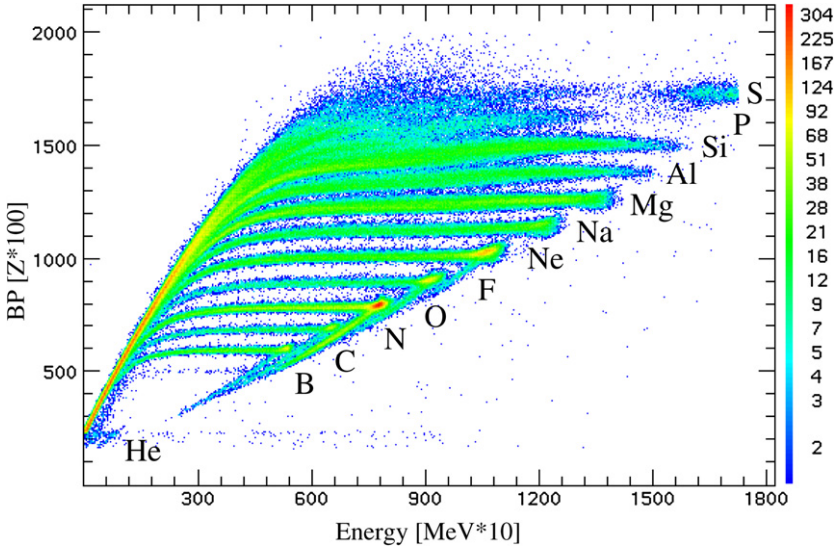


Fig. 3. A plot of energy, $E$, versus Bragg peak, $BP$, for BRS telescope 2. The horizontal scale is in MeV $\times$ 10 and the vertical scale $\approx Z \times 100$. The relative intensity ($\propto$ counts) is shown on the side bar. The different elements (labelled) are well separated enabling unambiguous $Z$ gates to be set. The end-point/punch-through energies for each element can be clearly seen.

the pre-amp module, and is treated separately in the subsequent analysis.) Following the gain-adjustment and summing of the BIC segment signals, they are matched to the position segments in case of multiple hits in the BICs caused by light charged particles, i.e. when two BIC segments fire, the segment used is that corresponding to the position signal. Next, a linear calibration was applied to the BIC signals on a run-by-run basis to correct for the accumulation of water vapour in the $CF_4$ counting gas. This effect steadily decreased the amplitudes of these signals; an effect of 11% over the course of the experiment.

In addition to the above corrections, a series of gates have been applied to the data. Of the events sorted, 94% are EUROBALL-only events as expected from the relative trigger rates in Section 2. BRS events with 'good' position and BIC signals comprise $\approx$1.3% of the data whereas further demanding a $\gamma$-ray in coincidence with a 'good' BRS event reduces the data to $\approx$0.2%. ('Good' position means that the BRS positions lie within the segment limits. 'Good' BIC means $BP$ and $E$ signals in the same segment as the position signals and that the BIC signals were such as to lie within a $Z$-gate i.e. on the $E$ versus $BP$ plot the $Z$ is unambiguous.)

Together with the above gates, events were also removed for which the total $Z$ ($Z_{\text{tot.}} = Z_1 + Z_2$) of the event was greater than the $Z$ of the compound system, i.e. $Z_{\text{tot.}} > 28$. These are primarily events for which $Z_{\text{tot.}}$ exceeds the $Z$ of the compound system by 4 units, i.e. mainly scattered beam particles entering the BRS telescopes in random coincidence. Of these events 99% are associated with $E_1 + E_2 > 165.4$ MeV, with many having twice the beam energy. These random coincidences contribute 4% to $Z_1$–$Z_2$ coincidences.

### 3.2. Gamma-ray analysis

Following the aforementioned treatment of the BRS data, the $\gamma$-ray data could be processed as outlined below.

After the energy calibration and alignment of the Ge time signals an 'addback' routine was employed to recover the full $\gamma$-ray energies for instances where multiple Ge crystals in one detector fired. For the 7-crystal cluster detectors, the energy signals from up to three neighbouring crystals were added together. (Note: the middle crystal is considered as a neighbour to all other crystals in the surrounding ring.) Similarly for the 4-crystal clover detectors, all of the energy signals from up to (any) three crystals were added together. When adding signals together, the angles of each crystal that fired were averaged in preparation for the Doppler-shift correction. The above procedure increased the full-peak efficiency by a factor of $\approx$1.4 for energies above $\sim$1 MeV.

The Doppler-shift correction part of the analysis fell into two parts, both of which use the following formula:

$$E_0 = E_{\text{lab.}}\left(\frac{1-(v/c)\cdot\cos\theta}{\sqrt{1-(v/c)^2}}\right) \tag{1}$$

where $E_{\text{lab.}}$ and $E_0$ are the observed and corrected $\gamma$-ray energies respectively, $\theta$ is the angle between the recoiling nucleus and the Ge detector, and $v$ is the recoil velocity. For those $\gamma$-events for which a BRS trigger was also recorded, the $\gamma$ rays were Doppler-shift corrected using the angle information (provided by the BRS position and Ge-detector angle), the energy signal ($E$) and $Z$ gates. To calculate the velocity from the energy signal, $N = Z$ was assumed for each element due to the absence of mass resolution in this measurement. (Note that the Doppler-shift correction for binary reactions (those without particle evaporation) could also be made using 2-body kinematics. The resulting FHWM for the $\gamma$ rays is the same as from the method used here.) For those events containing no BRS trigger, only EUROBALL data, the events were Doppler-shift corrected by assuming an average forward velocity of $v/c = 0.0615$. This velocity was obtained iteratively by minimising the peak widths in the final spectrum. Furthermore, in each case, the non-Doppler corrected energies were also stored to provide a check for the Ge-energy alignment and calibration via the intense 511 keV, $e^+e^-$ annihilation peak.

For the BRS-triggered $\gamma$ rays the FHWM is 17.5 keV (0.99%) at 1.8 MeV, whereas for the EUROBALL-only data the value is $\approx$23 keV (1.3–1.4%) at 1.8 MeV. This is a significant improvement given that a value of $<$1% has been achieved over a large angular range (out to 45.5°) and with multiple targets present in the form of oxygen/carbon in the target. A major contribution to this resolution remains the Ge opening angles. With the advent of segmented detectors combined with tracking algorithms this will lead to dramatic reductions in peak width under similar conditions.

After performing the above procedure using the graphical sorting-software DATA8M [15], the $\gamma$ rays were written out to a series of RadWare-format [8] histograms. Of these the following are of primary interest here:

$\gamma\gamma\gamma$: a 3-dimensional $\gamma$–$\gamma$–$\gamma$ cube containing Doppler-shift corrected $\gamma$ rays for which no BRS trigger was present.

brs-$\gamma\gamma$: a 2-dimensional $\gamma$–$\gamma$ matrix containing all Doppler corrected $\gamma$-ray events with BRS triggers.

brs-$\gamma$: 1-dimensional singles spectra for each BRS telescope containing all $\gamma$ rays with a BRS trigger.

The results from this analysis are discussed in the following section.

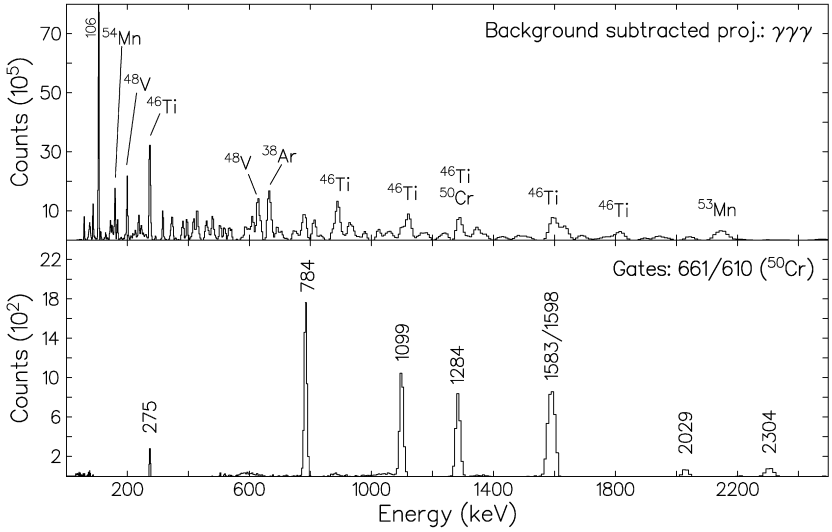


Fig. 4. Spectra from the EUROBALL-only data. (Top): background-subtracted total projection of the $\gamma\gamma\gamma$ cube; (bottom): background-subtracted spectrum, double gated by the 661 and 610 keV transitions in $^{50}$Cr. Transitions up to the $14^+$ state at 9917 keV can be identified. Note the different vertical scales.

## 4. Results

### *4.1. Euroball-only data*

Examining the various triggers recorded in the data, 94% of the events constitute EUROBALL-only (i.e. $\gamma$-only) data. The total projection of the $\gamma\gamma\gamma$ histogram is shown in Fig. 4 (top). Two of the most intense products are $^{46}$Ti and $^{50}$Cr isotopes corresponding to $2\alpha 2p$ and the $\alpha 2p$ evaporation channels respectively. Setting double gates on the $\gamma$-ray energies enables a very clean selection of a particular channel, the case for $^{50}$Cr is shown in Fig. 4 (bottom).

Of particular relevance to the discussion that follows is the distribution of isotopes identified in these data, and falls into three groups as shown in Fig. 5. The main population is from the $^{32}\mathrm{S} + {}^{24}\mathrm{Mg}$ reaction. The second, to the neutron-rich side of the vertical dashed line are products from reactions with aluminium in the target frame and are relatively weak. The third population starting with calcium and lighter isotopes is from oxygen and carbon (backing) in the $^{24}$Mg target. Examining the latter group of isotopes in more detail, it is apparent that the observed peaks lie systematically lower in energy than the literature values. E.g. for $^{41}$K, the 1677.2 keV transition [16] is observed at 1662 keV. This shift implies a Doppler correction using a higher velocity of $v/c \approx 0.08$ is required. From reactions on $^{24}$Mg, the average velocity appropriate for the dominant fusion–evaporation products with cleanly identified peaks was found to be $v/c = 0.0615$. In the current experiment the Ge detectors lie at predominantly backward angles; the average in-plane Ge angle is 115.57°. The higher velocity of $v/c \approx 0.08$ is consistent with fusion-evaporation reactions with a target $\sim$10 mass units lighter than $^{24}$Mg, half way between that for $^{16}$O (a shift of 8 mass units from $^{24}$Mg) and $^{12}$C (a shift of 12 mass units). Such data were not present in the $^{60}$Zn work [1,2], but here show a significant population of products from oxygen and carbon in the target, independent of the BRS results that follow.

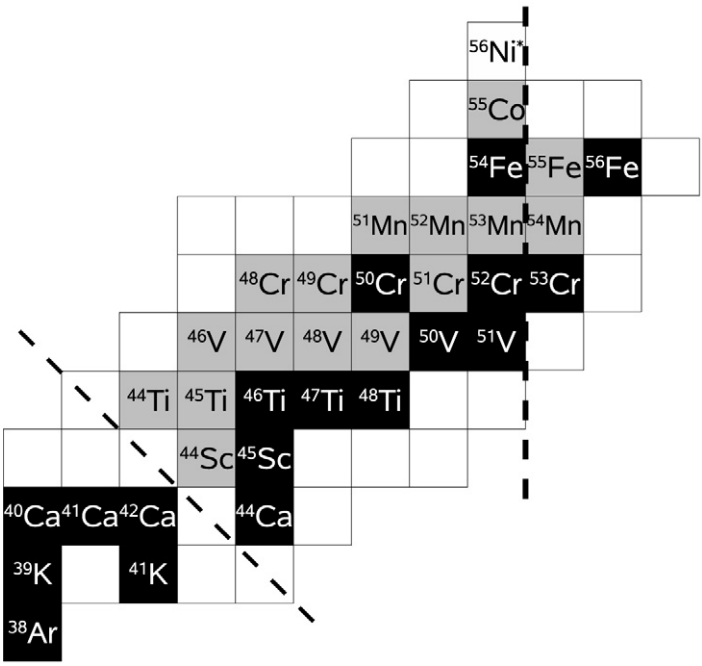


Fig. 5. Plot showing the isotopes observed in the EUROBALL-only data using a 'classic' Doppler correction ($v/c = 0.0615$). All of the labelled isotopes have been identified with the exception of the compound nucleus, $^{56}$Ni$^{\star}$, shown here only for orientation. Black squares indicate naturally abundant isotopes. See text for details.

### 4.2. BRS triggered data

Plotting $E$ versus $BP$ for each BRS telescope enabled a series of $Z$ gates to be set on the data to define the element for both the Doppler-shift correction and for separating the different product species. Following this step, the $\gamma$ rays for each product can be examined under various conditions. Examples of BRS-$\gamma$ coincidences are shown in Fig. 6. As can be seen, from the BRS-$\gamma$ projection (Fig. 6 (top)), the most prominent decays originate from deformed nuclei close to the target and/or beam nuclei. The most intense are $^{24}$Mg (target), $^{20}$Ne and $^{28}$Si (both from $\alpha$-particle transfer). At this point it is appropriate to comment on the cleanliness of the $Z$ separation. One of the most intense $\gamma$-ray transitions observed in these data is the 1779 keV $2^+ \rightarrow 0^+$ transition in $^{28}$Si, clearly seen in the Si-gate spectrum of Fig. 6 (middle). There is no leak-through of this line into the corresponding Al-gated spectrum of Fig. 6 (bottom)). Also, $\gamma$-decays of the order of tens of nanoseconds or less will appear as sharp lines in the spectra due to the $\approx$13 ns flight time to the front of the BRS. This is highlighted by the decay of the 417 keV $3^+$ state in $^{26}$Al with $t_{1/2} = 1.25 \pm 0.03$ ns [17], appearing as a sharp line in Fig. 6 (bottom).

Once the $\gamma$-ray data have established the clean separation of the products, the BRS telescopes can be used in coincidence to examine the out-of-plane angular correlations, relevant to a discussion of the evidence for hyper-deformation in Section 5. In particular, the $\phi_{1-2}(= \phi_1 - \phi_2)$ distributions as a function of 'missing' charge, $\Delta Z(= (Z_1 + Z_2) - 28)$ have been examined. Fig. 7 shows these out-of-plane distributions for all reaction channels, from true binary reactions with no 'missing' charge ($\Delta Z = 0$), up to reactions with $\Delta Z = -8$. As expected, for binary

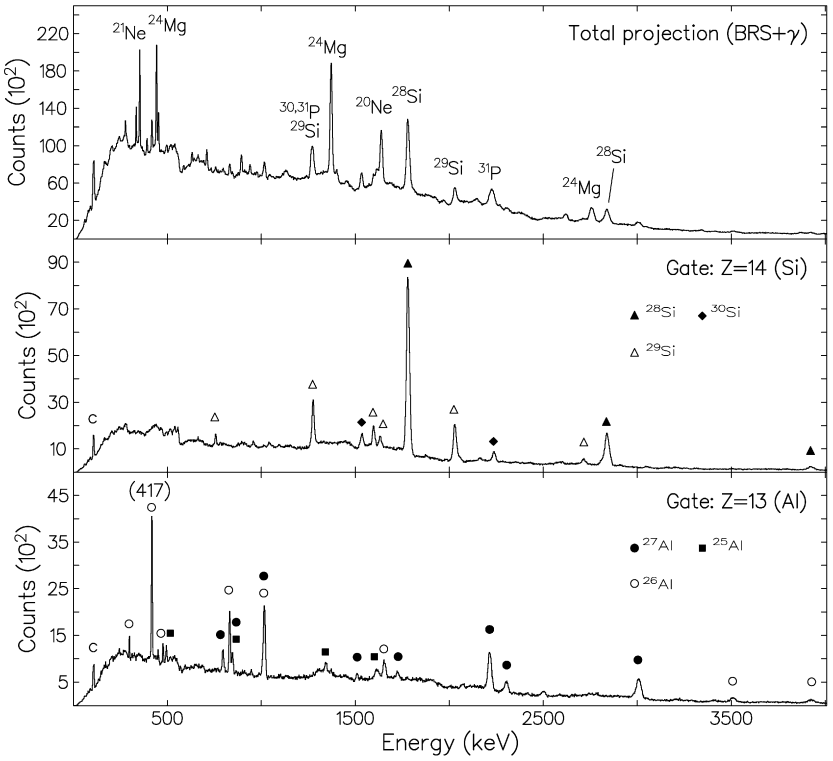


Fig. 6. BRS-gated spectra. (Top): full singles spectrum gated by BRS events with well-defined $Z$; (middle): spectrum gated by $Z = 14$ (silicon); (bottom): $Z = 13$ (aluminium) gated spectrum. The isotope(s) contributing to the most prominent peaks are indicated. In the bottom spectrum the 417 keV peak energy is also quoted. See text for details. Both $Z$-gated spectra represent the sum from gating on each BRS telescope. A contaminant from neutron activation in the Ge detectors is labelled 'c'.

reactions the products are coplanar, resulting in a sharp peak around 180°. As more particles are evaporated/emitted the distributions become broader as the products are no longer coplanar. However, for two of these distributions, namely $\Delta Z = -4$ and $-6$, the distributions are once more sharp, still peaked around 180°, though set on a broader background. The origin of these sharp components in the out-of-plane angular distribution forms the focus of the following section.

A further feature of the BRS data is the ability to define a binary reaction by setting two $Z$ gates; one on each BRS telescope. This enables the precise definition of a reaction. An added benefit is, following the definition of one $Z$-gate, the coincident $\gamma$ rays can be placed by successively changing the second $Z$-gate to isolate the parent of the transitions. By plotting the out-of-plane angular distribution versus $E_{\text{tot.}}$ $(= E_1 + E_2)$, the narrow out-of-plane component can be selected (Fig. 8 (inset)) in addition to the $Z$-gates. Projecting the resulting $\gamma$-ray spectra, for example in Fig. 8 for $Z = 9$ (F), enables the dominant coincident transitions to be isolated to $Z = 15$ (P) (as shown). This corresponds to the $\Delta Z = -4$ channel. An interpretation of this is the deuteron transfer channels from reactions on oxygen in the target.

These results are discussed in detail below.

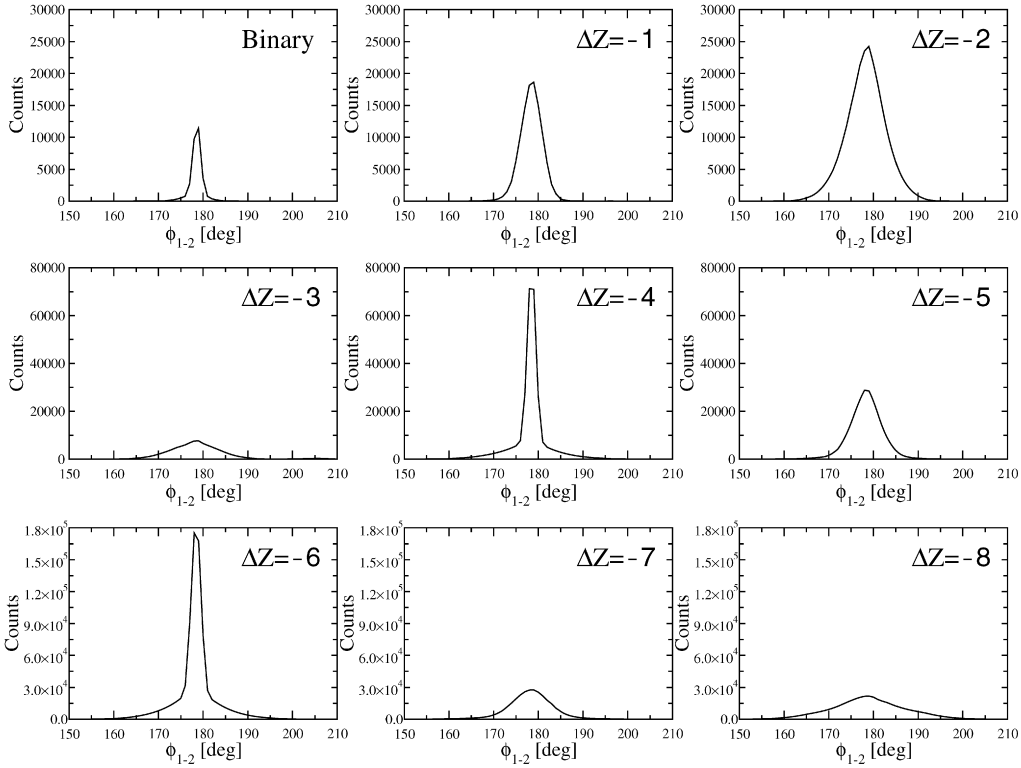


Fig. 7. Plot showing out-of-plane distributions, $\phi_{1-2}$ for BRS coincidences gated by 'missing' charge, $\Delta Z$. Note the different vertical scales for each row. Sharp correlations are observed for the $\Delta Z = -4$ and $-6$ channels. A systematic error of $-1.0^\circ$ is present in $\phi_{1-2}$.

## 5. Discussion

As set out in the introduction, recent claims for hyper-deformation in $^{60}$Zn [1,2] have been made based on closely related BRS data using a beam of $^{36}$Ar at 195 MeV incident on $^{24}$Mg. A similar analysis and interpretation of the current $^{56}$Ni data [4] has been completed making comparable claims. The particle–particle coincidences have been published and the out-of-plane correlations show the same pattern of broad and narrow peaks as in Fig. 7, namely that for the $\Delta Z = -4$ and $-6$ channels, the prominent feature of the distributions is a sharp peak around $180^\circ$. These distributions were first published in Ref. [12]. An important difference in the presentation of the distributions in Refs. [1,2,12] and Fig. 7 is that the earlier work shows only specific combinations of $Z$s contributing to a particular $\Delta Z$, not all possible combinations as shown here.

In the literature, four different interpretations have been discussed that could lead to this phenomenon.

(i) Elongated compound nuclear shapes (hyper-deformation), with multiple (or clusters of) $\alpha$-particles forming in the neck before fission occurs, as concluded in Refs. [1,2,4].
(ii) Pre-scission evaporation/emission, such that the out-of-plane correlations of the remaining fissioning system are undisturbed [12].

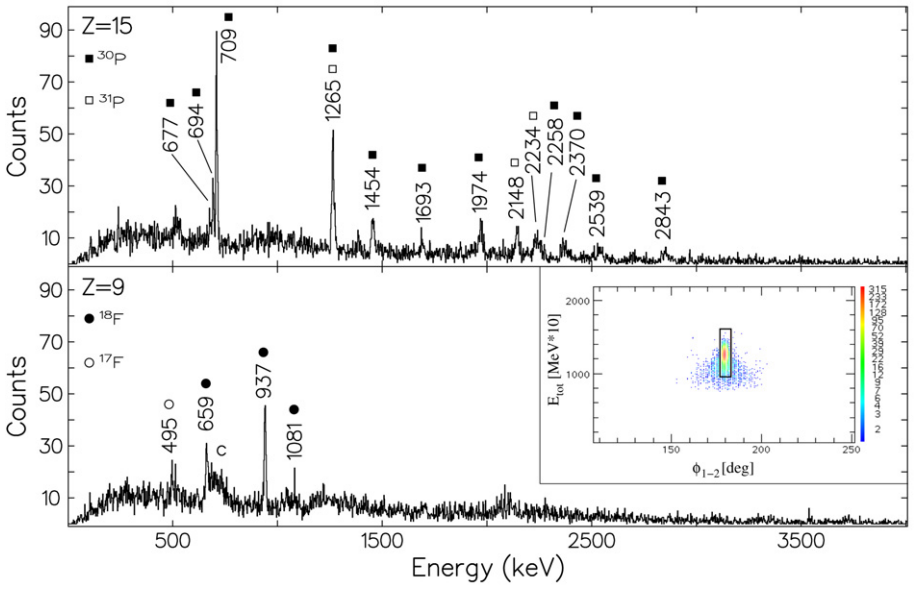


Fig. 8. Coincident $\gamma$-ray spectra generated by gating on the narrow component of the out-of-plane distribution (box in the inset) in the $\phi_{1-2}$ versus $E_{\text{tot.}}$ matrix. A rectangular gate from $177^\circ \rightarrow 183^\circ$ and including all energies above 95 MeV was used. Additionally, $Z = 9$ (fluorine) and 15 (phosphorus) gates in the BRS telescopes have been set (see spectra). A broad contaminant peak in the fluorine spectrum, indicated by 'c', arises from the strong coincident 709 keV transition in phosphorus being wrongly Doppler-shift corrected.

(iii) The emission of $\alpha$-particles with strongly aligned angular momentum vectors, such that they are emitted into the scattering plane of the two heavy products [12].
(iv) Reactions on oxygen and carbon in the $^{24}$Mg target simulating binary reactions with $\Delta Z = -4$ and $-6$ respectively [1,2,4].

Some discussion of the above points is necessary to clarify the merits/drawbacks of each proposal. (All four processes have been mentioned in Refs. [1,2,4].) In the first three processes, the 'missing' charge is assumed to be bound into $\alpha$-particles. For mechanism (i), the very negative $Q$-values for such ternary reactions (i.e. the $\Delta Z = -4$ and $-6$ channels) mean these reactions would only be able to compete with binary fission because of the contributions from the rotational energy at large angular momentum ($44\hbar$ [1,2]) and shell-corrections playing a role for such elongated shapes. However, there seems no a priori reason why only two and three $\alpha$-particles should exhibit this structure assuming highly deformed shapes.

The pre-scission evaporation of process (ii) is unlikely since the energy carried away by the $\alpha$-particles would be large, leaving insufficient energy for the subsequent fission process [18,19]. Also, if pre-scission were responsible, the $\Delta Z = \textit{odd}$ channels would also exhibit these out-of-plane correlations.

Process (iii) requiring strongly aligned angular momentum vectors is discounted in Refs. [1, 2] because no sharp out-of-plane correlations are observed in the $1\alpha$ channel. This process also seems unlikely as it is difficult to imagine the mechanism behind it.

Regarding process (iv), whilst such a scenario has been discussed in Refs. [1,2,4] it was reported to be unable to produce sufficient yields in the relevant reaction channels. This conclusion

Table 1
Yields ($\times 10^6$ counts) as a function of $\Delta Z$ for the out-of-plane distributions shown in Fig. 7. For the $\Delta Z = -4$ and $-6$ cases, the number of counts in the narrow component of the $\phi_{1-2}$ distributions are also given

| $\Delta Z$ | 0 | −1 | −2 | −3 | −4 | −5 | −6 | −7 | −8 |
|---|---|---|---|---|---|---|---|---|---|
| Yields (all) | 0.03 | 0.11 | 0.24 | 0.09 | 0.27 | 0.23 | 0.78 | 0.30 | 0.39 |
| Yields (narrow) | – | – | – | – | 0.21 | – | 0.58 | – | – |

was reached after a quantitative comparison of the fission yields on $^{24}$Mg and then by assuming that these differential cross-sections will remain the same for reactions on an $^{16}$O target. This analysis was carried out for several reaction channels. Resulting from this, the estimated oxygen contents of the magnesium targets are ≈45% in the $^{56}$Ni [4] data and ≈15% in the $^{60}$Zn experiment [1,2]. (*As mentioned earlier, a difference in the oxidation levels is expected due to the different target handling procedures. The target for the $^{60}$Zn experiment* (100 μg/cm$^{-2}$ $^{24}$*Mg backed with* 20 μg/cm$^{-2}$ *carbon*) *was transferred under vacuum whereas the $^{56}$Ni target was stored and transported to the chamber unprotected. The vacuum quality in the target chamber was also significantly worse during the $^{56}$Ni experiment, being* $\sim 10^{-3}$ mbar.) However, the $Q$-values, thresholds and centre-of-mass energies are different for reactions on $^{16}$O and indeed for $^{12}$C too. An independent way of obtaining these yields would be to run the experiment using pure $^{16}$O and $^{12}$C targets, without $^{24}$Mg, as is routinely done in other charged-particle spectroscopy measurements.

For the current work, the yields corresponding to Fig. 7 are given in Table 1. The binary, $\Delta Z = -4$ and $-6$ channels all show sharp distributions peaked around 180°, set on a broader background. This broad background, is interpreted here, as for the $^{60}$Zn data [1,2], as originating from reactions on $^{24}$Mg with increasing numbers of particles emitted/evaporated. In addition to the presence of a narrow component in the $\phi_{1-2}$ distributions, the highest yields are also observed for the $\Delta Z = -4$ and $-6$ channels. This is markedly different from the $^{60}$Zn reaction in which the yield peaks at $\Delta Z = -1$. This is again an indication of the lower target contamination. The relative yield in the $^{60}$Zn for $\Delta Z = -4$ compared to binary is $<1$ whereas for the present data the products from oxygen dominate. In addition to the large oxygen content the results are indicative of carbon build-up on the target in the present work, most likely resulting from the poor vacuum of $\sim 10^{-3}$ mbar during the experiment.

In Table 2 the yields for the different even-$\Delta Z$ channels are given as a function of $Z$, side-by-side with the relevant $Q$-values. The yields for the narrow component of the $\Delta Z = -4$ and $-6$ channels are obtained by gating on a $\phi_{1-2}$ versus $E_{\text{tot.}}$ plot. Firstly, it is worth pointing out that the ternary reactions have highly negative $Q$-values, 14.05 MeV and 21.21 MeV *more negative* than the corresponding reactions on $^{16}$O and $^{12}$C respectively. Shell-correction energies [20] and rotational energies are each calculated to be ∼5 MeV for a hyper-deformed $^{56}$Ni$^{\star}$ nucleus and are insufficient to explain the large yields.

Looking in more detail at the narrow distributions for each element, the $\alpha$-transfer reaction is the most intense for each $\Delta Z$. The elastic scattering contribution is also significant, being the second most intense channel for all but $\Delta Z = -4$ (see below). This dominance of $\alpha$-transfer is likely due to the BRS acceptance. By 12.5° the Rutherford-scattering cross-section has decreased by five orders of magnitude for reactions on all three targets. In all cases, again assuming target contaminants play a major role, the $2\alpha$-transfer also has significant yield. In the binary case, this contributes to the elastic channel, for $\Delta Z = -2$, $2\alpha$-transfer contributes to the $1\alpha$-transfer yields and for $\Delta Z = -4$ ($-6$) $2\alpha$-transfer is the second (third) most intense channel. In other words

Table 2
Distributions of binary reaction products by $Z$, assuming $N = Z$ isotopes. Ground-state $Q_0$-values for each reaction are also quoted in MeV. For the $\Delta Z = -4$ and $-6$ reactions, the $Q_0$-values are quoted assuming reactions on target contaminants $^{16}$O and $^{12}$C respectively. The corresponding ternary-reaction $Q_0$-values are 14.05 MeV and 21.21 MeV more negative for $\Delta Z = -4$ and $-6$ respectively. Only the narrow component of the $\phi_{1-2}$ distributions are considered for $\Delta Z = -4$ and $-6$. Products heavier than Cl could not be cleanly separated in this experiment. The $\alpha$-transfer channels for each $\Delta Z$ are shown in bold, with elastic channels in italics

| $Z$ | | $Z$ distributions | | | | | | | |
|---|---|---|---|---|---|---|---|---|---|
| | | Binary | | $\Delta Z = -2$ | | $\Delta Z = -4$ (narrow) | | $\Delta Z = -6$ (narrow) | |
| | | Cnts | $Q_0$ | Cnts | $Q_0$ | Cnts | $Q_0^{^{16}\mathrm{O}}$ | Cnts | $Q_0^{^{12}\mathrm{C}}$ |
| 5 | (B) | – | – | – | – | – | – | 53 | −13.63 |
| 6 | (C) | – | – | – | – | – | – | *69063* | *0.00* |
| 7 | (N) | – | – | – | – | 279 | −9.18 | 54852 | −8.68 |
| 8 | (O) | – | – | – | – | *40380* | *0.00* | **359155** | **+0.21** |
| 9 | (F) | – | – | 97 | −18.81 | 29411 | −11.43 | 25694 | −14.68 |
| 10 | (Ne) | – | – | 49359 | −9.32 | **81777** | **−2.22** | 61908 | −5.04 |
| 11 | (Na) | 20 | −10.33 | 17890 | −16.99 | 23751 | −13.36 | 14662 | −15.65 |
| 12 | (Mg) | *16165* | *0.00* | **157233** | **−6.95** | 61146 | −2.89 | 61908 | −5.04 |
| 13 | (Al) | 4205 | −7.54 | 29452 | −17.95 | 23751 | −13.36 | 25694 | −14.68 |
| 14 | (Si) | **22300** | **+3.04** | **157233** | **−6.95** | **81777** | **−2.22** | **359155** | **+0.21** |
| 15 | (P) | 4205 | −7.54 | 17890 | −16.99 | 29411 | −11.43 | 54852 | −8.68 |
| 16 | (S) | *16165* | *0.00* | 49359 | −9.32 | *40380* | *0.00* | *69063* | *0.00* |
| 17 | (Cl) | 20 | −10.33 | 97 | −18.81 | 279 | −9.18 | 53 | −13.63 |

the yields can be qualitatively understood for all even $\Delta Z$s in terms of target contaminants and $\alpha$-transfer (with favoured $Q$-values) and elastic-scattering reactions. All show the same trend. One last point of interest is the odd-even staggering in the yields, with the odd-$Z$ products having the most negative $Q$-values and consequently their yields are suppressed compared to the even-$Z$ neighbours. For ternary reactions, without considering oxygen and carbon as targets, the yields are difficult to understand. In particular it is not clear why the $\Delta Z = -6$ channel would be so much favoured given the large negative $Q$-values. In such a scenario the $\Delta Z = -4$ and $-2$ should be more intense.

Turning now to the $^{60}$Zn experiment, there are some distinct differences. Considering the $Q$-values once more, $\alpha$-transfer is again favoured for binary reactions with $Q_0 = +3.34$ MeV. For $\Delta Z = -2$ and $-4$ the values are similar to those in the $^{56}$Ni case, but with the $2\alpha$-transfer now favoured ($Q_0 = -3.60$ MeV) over the $1\alpha$-transfer ($Q_0 = -6.64$ MeV). Finally for $\Delta Z = -6$, the $1\alpha$-transfer is has a small positive $Q$-value (+0.52 MeV), with $2\alpha$-transfer having $Q_0 = -1.70$ MeV. The yields in Refs. [1,2] are presented differently to Table 2 here, with the $\phi_{1-2}$ distributions being shown for only a few selected pairs of $Z$s. However, the differential cross-sections are extracted as a function of $\Delta Z$ which also show the odd-even staggering. For binary reactions, the cross-sections are highest for $^{28}$Si and $^{32}$S ($1\alpha$-transfer) and $^{36}$Ar and $^{24}$Mg (elastic). For $\Delta Z = -2$, the partitions with the most strength again correlate with the $Q$-values, peaking at $^{28}$Si ($2\alpha$-transfer) as expected, but with significant strength in the $1\alpha$-transfer combination. For the $\Delta Z = -4$ ($-6$) reactions the peak yields are for $^{24}$Mg and $^{28}$Si ($^{24}$Mg and also $^{28}$Si and $^{20}$Ne), again correlating with the $Q$-values calculated assuming target contaminants. Unfortunately, the coincident yields for the $1\alpha$-transfer with $\Delta Z = -6$ ($^{32}$S and $^{16}$O) were not measurable in the $^{60}$Zn data. To summarise the above findings, for the $^{60}$Zn data too, there is a correlation between relative yields for a given $\Delta Z$ and $Q$-value with $\alpha$-transfer dominating.

Also, the overall yields are compatible with oxygen and also a smaller amount of carbon consistent with the known target backing.

Returning to the current $\gamma$-ray data, in addition to isolating coincidences between, for example, $Z = 9$ (F) and 15 (P) (Fig. 8), interpreted as proton and deuteron transfer on an oxygen target, the spectra have been used to examine spin distributions of binary partner events. This was performed to see if there is a different spin population for nuclei populated in reactions on the $^{24}$Mg target compared to the target contaminants. This was undertaken by plotting, for example for $^{28}$Si, the $\gamma$-ray yield ratio: $\frac{I_\gamma(4_1^+ \rightarrow 2_1^+)}{I_\gamma(2_1^+ \rightarrow 0_1^+)}$ as a function of binary partner, i.e. $Z$. However, within the uncertainties a constant ratio was observed, the weighted mean of which is $0.27 \pm 0.01$. Similarly for transitions in $^{29}$Si, no significant change in spin population has been observed as the partner $Z$ is varied. This is perhaps not surprising since the $\gamma$ rays examined here are from relatively low-spin states and are therefore easily populated in both the $^{32}\mathrm{S} + {}^{24}\mathrm{Mg}$ reactions and the reactions on $^{16}$O and $^{12}$C.

It is striking that the only sharp distributions after the binary reaction channel are those corresponding to target contaminants. Products from target contaminants lighter than magnesium have been observed in the EUROBALL-only data (Fig. 5); confirmed by the shift seen in the Doppler correction necessary to reproduce the published transition energies (Section 4.1). The small sharp peak in the out-of-plane correlation reported in Refs. [1,2] for the $\Delta Z = -8$ channel is not seen here (see Fig. 7). Furthermore, this phenomenon has only been observed using $^{24}$Mg targets. It would be elucidating to perform experiments using a similar detector set-up but with different beam and target combinations to firmly tie down the mechanism responsible.

Whilst the present analysis does not preclude a small contribution from ternary fission processes, no evidence is found making it necessary to invoke such an argument.

## 6. Summary

In summary, data taken in coincidence with the EUROBALL Ge detector array and the Binary Reaction Spectrometer have been presented for binary reactions between $^{32}$S projectiles and a $^{24}$Mg target. The case for hyper-deformation has been examined in both the current data and previously published work utilising the BRS relating to $^{60}$Zn. In contrast to the published BRS data showing tentative evidence for such an effect in $^{60}\mathrm{Zn}^\star$, the data here for $^{56}\mathrm{Ni}^\star$ are interpreted as being compatible with target contaminants. The observation in the EUROBALL-only data of fusion-evaporation products from a target with $A \sim 14$ suggest that both carbon and oxygen are present in appreciable quantities. Furthermore, the yields relating to narrow out-of-plane correlations have been examined and the population systematics found to be consistent across all three targets (Mg, O and C), with $\alpha$-transfer and elastic scattering reactions dominating, correlated with their favourable $Q$-values. The earlier study of $^{60}$Zn has also been discussed and the published yield patterns understood in terms of the same dominant reaction channels and favourable $Q$-values. The striking difference between the two experiments in the absolute yields in the different channels is attributed to the different target handling.

## Acknowledgements

The authors would like to thank the Vivitron accelerator staff for the sulphur beam. Clausi Beschorner is thanked for their numerous contributions to the graphical sorting software. G. Duchêne, F. Haas and D.G. Jenkins are thanked for their contribution to part of the data

collection. C.W. is grateful for the support of the Alexander von Humboldt Foundation and an STFC Advanced Research Fellowship. Tz.K. acknowledges a DAAD scholarship.

## References

[1] V. Zherebchevsky, W. von Oertzen, D. Kamanin, B. Gebauer, S. Thummerer, Ch. Schulz, G. Royer, Phys. Lett. B 646 (2007) 12;
V. Zherebchevsky, W. von Oertzen, D.V. Kamanin, JETP Lett. 85 (3) (2007) 136.
[2] W. von Oertzen et al., Phys. Rev. C, submitted for publication.
[3] R.M. Lieder, H. Jäger, A. Neskakis, T. Venkova, Nucl. Instrum. Methods Phys. Res. 220 (1984) 363.
[4] W. von Oertzen, et al., Eur. Phys. J. A 36 (2008) 279.
[5] B. Gebauer, et al., in: W. Gelletly, et al. (Eds.), Proceedings of the International Conference on the Future of Nuclear Spectroscopy, Crete, Greece, National Technical University Press, Athens, 1993, p. 168.
[6] B. Gebauer, et al., in: W. Korten, S. Lunardi (Eds.), Achievements with the Euroball Spectrometer, 2003 p. 135, Scientific and technical activity report, available on-line at: http://euroball.lnl.infn.it/EBmore/EB_Final_Report.pdf.
[7] F. Ajzenberg-Selove, Nucl. Phys. A 506 (1990) 1.
[8] D.C. Radford, Nucl. Instrum. Methods Phys. Res. A 361 (1995) 297.
[9] H.J. Wollersheim, D.E. Appelbe, A. Banu, R. Bassini, T. Beck, F. Becker, P. Bednarczyk, K.-H. Behr, M.A. Bentley, G. Benzoni, C. Boiano, U. Bonnes, A. Bracco, S. Brambilla, A. Brünle, A. Bürger, K. Burkard, P.A. Butler, F. Camera, D. Curien, J. Devin, P. Doornenbal, C. Fahlander, K. Fayz, H. Geissel, J. Gerl, M. Górska, H. Grawe, J. Gręboszc, R. Griffiths, G. Hammond, M. Hellström, J. Hoffmann, H. Hübel, J. Jolie, J.V. Kalben, M. Kmiecik, I. Kojouharov, R. Kulessa, N. Kurz, I. Lazarus, J. Li, J. Leske, R. Lozeva, A. Maj, S. Mandal, W. Męczyński, B. Million, G. Münzenberg, S. Muralithar, M. Mutterer, P.J. Nolan, G. Neyens, J. Nyberg, W. Prokopowicz, V.F.E. Pucknell, P. Reiter, D. Rudolph, N. Saito, T.R. Saito, D. Seddon, H. Schaffner, J. Simpson, K.-H. Speidel, J. Styczeń, K. Sümmerer, N. Warr, H. Weick, C. Wheldon, O. Wieland, M. Winkler, M. Zięblíński, Nucl. Instrum. Methods A 537 (2005) 637.
[10] B. Gebauer, et al., Nucl. Instrum. Methods Phys. Res. A, submitted for publication.
[11] Ch. Schulz, Diploma Thesis, Hahn-Meitner-Institut and Technische Universität, Berlin (1995).
[12] S. Thummerer, B. Gebauer, W. von Oertzen, M. Wilpert, Nuovo Cimento A 111 (8–9) (1998) 1077.
[13] S. Thummerer, PhD Thesis, Hahn-Meitner-Institut and Freie Universität, Berlin (1999), URL: http://www.diss.fu-berlin.de/2000/14/indexe.html.
[14] S. Thummerer, B. Gebauer, H.G. Bohlen, W. von Oertzen, D. Bazzacco, S.M. Lenzi, A. Algora, G. de Angelis, A. Gadea, D.R. Napoli, C. Borcan, F. Dönau, L. Käubler, H. Schnare, R. Schwengner, I. Peter, C. Beck, C. Bhattacharya, M. Rousseau, R. Nouicer, J. Lisle, Phys. Scr. T 88 (2000) 114.
[15] DATA8M graphical sorting software, Martin and Thomas Wilpert, Hahn-Meitner-Institut (1996) unpublished. Extensively updated by Clausi Beschorner and Severin Thummerer, Hahn-Meitner-Institut, URL: http://www.hmi.de/people/beschorner/data8m/html/data8m.html.
[16] F. Jundt, E. Aslanides, A. Gallman, E.K. Warburton, Phys. Rev. C 4 (1971) 498.
[17] C.R. Gould, D.R. Tilley, N.R. Roberson, Phys. Rev. C 7 (1973) 1068, and references therein.
[18] T. Matsuse, C. Beck, R. Nouicer, D. Mahboub, Phys. Rev. C 55 (1997) 1380.
[19] S.J. Sanders, A. Szanto de Toledo, C. Beck, Phys. Rep. 311 (1999) 487.
[20] I. Ragnarsson, S. Åberg, R.K. Sheline, Phys. Scr. 24 (1981) 215.